EPJ Web of Conferences **114**, 02040 (2016)
DOI: 10.1051/epjconf/201611402040

The use of wind tunnel facilities to estimate hydrodynamic data

Kristoffer Hoffmann[1,a], Johannes Tophøj Rasmussen[1], Svend Ole Hansen[1], Marit Reiso[2], Bjørn Isaksen[3], and Tale Egeberg Aasland[4]

[1] Svend Ole Hansen ApS, Copenhagen, Denmark
[2] Reinertsen AS, Trondheim, Norway
[3] Norwegian Public Roads Administration, Oslo, Norway
[4] Norwegian Public Roads Administration, Stavanger, Norway

Abstract. Experimental laboratory testing of vortex-induced structural oscillations in flowing water is an expensive and time-consuming procedure, and the testing of high Reynolds number flow regimes is complicated due to the requirement of either a large-scale or high-speed facility. In most cases, Reynolds number scaling effects are unavoidable, and these uncertainties have to be accounted for, usually by means of empirical rules-of-thumb. Instead of performing traditional hydrodynamic measurements, wind tunnel testing in an appropriately designed experimental setup may provide an alternative and much simpler and cheaper framework for estimating the structural behavior under water current and wave loading. Furthermore, the fluid velocities that can be obtained in a wind tunnel are substantially higher than in a water testing facility, thus decreasing the uncertainty from scaling effects.
In a series of measurements, wind tunnel testing has been used to investigate the static response characteristics of a circular and a rectangular section model. Motivated by the wish to estimate the vortex-induced in-line vibration characteristics of a neutrally buoyant submerged marine structure, additional measurements on extremely lightweight, helium-filled circular section models were conducted in a dynamic setup. During the experiment campaign, the mass of the model was varied in order to investigate how the mass ratio influences the vibration amplitude. The results show good agreement with both aerodynamic and hydrodynamic experimental results documented in the literature.

1 Introduction

Vortex-induced vibrations (VIV) of cylinders is a widely studied phenomenon due to its relevance in numerous engineering disciplines. Several reviews have been written on the matter of VIV of circular cylinders [1–3], as well as the more complicated cases of interference between two closely separated cylinders [4] and the structural instabilities of rectangular cylinders [5].

A series of wind tunnel test has been performed to investigate the response characteristics of different cylinder cross sections. The objective of the tests is to provide necessary key parameters for the initial design of a submerged floating tube bridge (SFTB) under consideration for the Bjørnafjord crossing south of Bergen, Norway. At the current stage in the design process, the use of wind tunnel testing, as opposed to hydrodynamic testing, is a great advantage.

Investigation of vortex-induced structural oscillations in hydrodynamic laboratories is time-consuming and expensive. In addition, the results will have an inherent uncertainty due to Reynolds number scaling effects. Similarity in Reynolds number is exceedingly hard to achieve in a water setup, as it requires either a large-scale setup or very high fluid velocities. The latter situation will also induce very large forces on the model structure. In a wind tunnel, these effects are less prominent, as the fluid velocities that can be obtained are substantially higher than in a water testing facility and the inertial forces are much smaller. Wind tunnel experiments allow Reynolds numbers in the range of the resonance wind velocities ($10^4 \leq Re \leq 10^6$), which also gives a good basis for predicting the behaviour in full scale. This, along with the relative ease of the setup and the reduction in cost, makes the use of wind tunnel testing to determine hydrodynamic data an attractive alternative to water facility testing.

Wind tunnel facilities are widely used in the investigation of vortex dynamics and the related structural issues, and numerous studies of VIV and flow instabilities of cylinders have been carried out in wind tunnels. What these studies have in common, is that they operate with comparatively large mass ratios. For instance, a recent study [6] of VIV on circular cylinders in the post-critical regime refers to a mass ratio of 35 as ”quite low with respect to tests in air”. A widely sited master’s thesis work [7] employs a mass ratio of approximately 250 for wind tunnel experiments. However, for neutrally buoyant structures submerged in water the mass ratio is typically of order 1, and at such low mass ratios the scientific literature does not seem to cover wind tunnel experiments characterising the vortex-induced structural dynamics.

Mass and damping have a significant effect on VIV, and in order to obtain a realistic result for the present study, this must be taken into account. The effect of mass and damping on VIV for a circular cylinder has been investigated numerically, and it was found that variations of the mass and damping ratios have almost the same result on the system

[a] e-mail: kho@sohansen.dk

response. Increasing the mass ratio will reduce the maximum amplitude, and also the velocity range over which lock-in occurs [8]. This corresponds to earlier findings [9], where experiments with the same mass-damping parameter were carried out in both air and water. In the present investigation, lightweight helium-filled models have been used for the dynamic tests, in order to get model mass ratios that simulate neutral buoyancy in water.

2 Existing theories and methodologies

Vortex-induced vibrations are described mathematically by a number of models of the physics behind vortex formation, the associated oscillating loads and the structural dynamics, incorporating the associated coupling of these phenomena. The physical parameters and principles allow for the formulation of response models used to establish general design criteria primarily related to structural vibrations.

2.1 Determining parameters and basic principles

A number of basic non-dimensional parameters have been established to describe and characterise the main static and dynamic behaviour of structures subjected to in-line and cross-flow vortex-induced vibrations. These parameters depend on relevant structural and flow-specific properties.

The specific unique ratio of inertial and viscous forces is given by the Reynolds number, defined by the well-known expression

$$Re = \frac{UD}{\nu}, \tag{1}$$

where U is the mean velocity of the undisturbed flow, D is the cross-flow structural dimension and ν is the kinematic viscosity of the fluid.

The ratio between the oscillating mass of the structure, being in the model or full-scale configuration, and the mass of the equivalent displaced fluid can be expressed by the mass ratio

$$\lambda = \frac{m_{\text{osc,structure}}}{m_{\text{osc,fluid}}}. \tag{2}$$

Note that this is a purely structural parameter. In this expression $m_{\text{osc,structure}}$ denotes the complete mass of all oscillating parts. For both the numerator and the denominator, the oscillating mass of the surrounding fluid is in this paper approximated by the mass of the displaced fluid. For example, a structure having the same density as the surrounding fluid, will have a mass ratio of 1. A structure with twice the density of the surrounding fluid, will have a mass ratio of 3/2, since the density of the oscillating surrounding fluid reamins unchanged.

The Strouhal number is defined by the well-established relation

$$St = \frac{n_s D}{U}, \tag{3}$$

where n_s is the frequency of the lateral loads. A similar relationship is defined in oscillatory flow, where the relative orbital motion of fluid particles relative to the characteristic length of the immersed object plays a crucial role. This relationship is expressed by the Keulegan–Carpenter number [10].

For the present analysis, the structural susceptibility to vortex-induced vibrations is characterised by the general mass-damping parameter

$$Sc_G = \frac{2\delta_s m_e}{\rho L D}. \tag{4}$$

In the formula above, δ_s is the structural damping quantified by the logarithmic damping decrement in still fluid, m_e is the equivalent mass per unit length corresponding to the mode considered, ρ is the density of the surrounding fluid, and L is the in-line structural dimension. The presented expression is a generalisation of the Scruton number, taking into account structures having a non-circular cross-sectional geometry [11]. Note that in the case of a structure exposed to vortex shedding along its complete extension, the mass-damping parameter is simply a damping term multiplied by the ratio between the density of the oscillating structural mass and the density of the surrounding fluid.

The structural response is described in terms of a fundamental relation between the reduced fluid velocity and the reduced amplitude. The reduced fluid velocity is in relation to in-line vibrations defined by

$$U_r = \frac{U}{n_e D}, \tag{5}$$

where n_e is the in-line natural frequency of the structure in still fluid, and the reduced amplitude is defined by

$$A_r = \frac{A}{D}, \tag{6}$$

where A is the amplitude of the in-line oscillation.

It should be noted that the use of the reduced velocity as the parameter characterising the in-line vibrational response may not be optimal, at least for very low mass ratio structures. It seems reasonable that the forcing frequency caused by vortex shedding is dependent on the actual oscillation frequency and not the natural frequency of the structure in a still fluid. For cross-flow oscillations, the velocity normalised by the actual oscillation frequency has been shown to give a better description of the experimental data in some situations [12]. However, in the present paper, the reduced velocity is used as the descriptive parameter, since this is in accordance with the majority of the literature and design codes related to in-line oscillations.

The basic physical principles of vortex shedding induce an oscillating drag force which drive in-line structural oscillatory vibrations. Two different scenarios can occur, both corresponding to alternating low-pressure vortices on the downstream side of the object. Normal vortex shedding combined with a secondary, symmetric vortex shedding, which occurs as a result of in-line structural motion relative to the fluid, can create downstream pressure variations oscillating with a frequency of approximately three times the Strouhal frequency. This mechanism is responsible for the first fluid instability causing in-line vibrations. The second fluid instability causing in-line vibrations occur for slightly larger fluid velocities, where the forcing is entirely due to normal vortex shedding. Since the shedding is limited to low-pressure vortices on the downstream side of the object, the forcing frequency in the in-line direction is approximately twice the Strouhal frequency. It should

also be mentioned, that since vortex-induced in-line vibrations in steady flow occur at relatively low fluid velocities, the oscillation amplitudes are in the order of one magnitude smaller than the corresponding cross-flow vibrations usually experienced at larger flow velocities [10].

2.2 In-line amplitude response models

Structural vibrations caused by vortex-induced oscillating loads can be described in a simplified fundamental mathematical framework, based on theoretical and experimental research in the oscillating fluid/structure interaction, combined with general accepted experience from the construction and operation of different types of structures susceptible to VIV. To a certain extent, experiments in fluid dynamic testing facilities has also helped to clarify and specify certain aspects of this description.

A fundamental description of the in-line reduced amplitude response for submerged cylindrical structures in flowing water can be given in terms of the reduced fluid velocity and a mass-damping parameter. Experiments, such as those performed by King [13], have verified the presence of two fluid instability regions and in broad terms defined the associated in-line response amplitude characteristics.

Det Norske Veritas (DNV) has developed application-based design criteria and recommendations for free-span submarine pipelines which prescribe in-line response curves based on the reduced velocity and a stability parameter similar to the mass-damping parameter, but taking into account to total modal damping [14]. The in-line response model covers both fluid instability regions, corresponding to symmetric and regular, asymmetric vortex shedding for a uniform mode shape. The DNV model is used as a reference guideline for the maximum in-line response of cylindrical low mass ratio structures submerged in steady flowing water; thus, together with the wind tunnel measurements it is used to compare the response characteristic measured for low mass ratio structures in steady air with those expected for similar low mass ratio structures submerged in steady flowing water.

In its general description, the maximum reduced in-line amplitude response for neutrally buoyant cylindrical structures submerged in steady flowing water is similar to the principal sketch in figure 1. In King's laboratory testing with an oscillation given by a free-end mode shape, the two instability regions are clearly visible. The DNV specifications are similar, but more general and the response covers are larger area, especially for $U_r > 3$. The DNV model is in figure 1 presented for a stability parameter of 0.2. At higher levels of total damping, the onset reduced velocity is increased slightly and the maximum response is decreased. The reduced velocity above which in-line vibrations are insignificant is also lowered. Note that the response models only describe the response caused by in-line VIV, and other phenomena, such as galloping or torsional structural instabilities, may change the actual response significantly.

The ultimate goal of the present analysis is to determine if the known dynamic behaviour of neutrally buoyant structures in steady flowing water, expressed by the presented in-line response models, is similar to the dynamics of neutrally buoyant model structures in air.

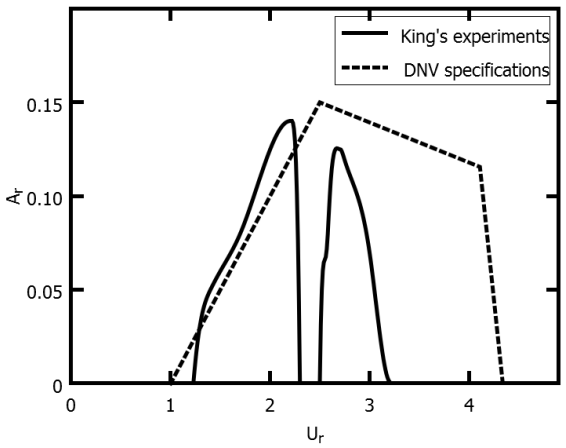

Figure 1: Principal sketch of the maximum reduced in-line amplitude response as a function of the reduced fluid velocity for low mass ratio cylindrical structures submerged in steady flowing water. The presented general response characteristics are based on published results from laboratory experiments in water for a free-end mode shape [13] ($Re = 6 \times 10^4$) and a response model from code specifications for a uniform mode shape, assuming a stability parameter of 0.2 [14].

2.3 Experiences and common practice when designing submerged marine structures

Vortex-induced vibrations are a key issue in many disciplines of marine engineering design. Currently defined response models, as those presented previously, are used to give overall indications of the onset and intensity of both in-line and cross-flow VIV. Certain structure-specific properties, such as the cross section geometry, inter-structural spacing and the distance to any flow boundaries may, however, influence the response significantly [15]. Hydrodynamical tests are as a natural consequence used to investigate the possibility of structural behaviour not covered by existing response models, such as for instance was the case with the initial studies performed at the Norwegian Marine Technology Research Institute (MARINTEK) in connection with the proposed Høgsfjord SFTB crossing and the Ormen Lange pipeline project.

The motivation for the present study is to investigate if one can use wind tunnel experiments, as an alternative to hydrodynamic experiments, to obtain information of the hydrodynamic behaviour of cross sections relevant for submerged floating tube bridges. The procedure will also provide valuable indications of how to utilise wind tunnel experiments to link the aerodynamic and hydrodynamic data base closer together and describe a fundamental methodology for the transfer of certain aerodynamic actions to equivalent hydrodynamic actions.

3 Experimental design and setup

The performed experimental testing includes measurements of static and dynamic flow-induced model responses performed in wind testing facilities at Svend Ole Hansen ApS, Copenhagen, Denmark and SOH Wind Engineering LLC,

Vermont, USA. In the following section, the experimental methodologies of the static and dynamic measurements are outlined and the geometric properties of the analysed cross section models are presented.

3.1 Testing procedure

All conducted model tests are twofold: Tests in the static rig provide data to estimate the drag coefficient C_D, and the lift and moment coefficients C_L, C_M, together with their angular derivatives, which enable a description of fluid-induced forces and the aeroelastic or hydroelastic characteristics of the structure. Spectral analyses of the drag and lift signals provide an additional insight into the oscillating flow mechanisms for the fixed structure. This is described by the Strouhal number for cross-flow vortex-induced oscillations. Tests in the dynamic rig provide data used to predict the risk of flow-induced vibrations, especially vortex-induced in-line vibrations of the structure. Different degrees of spring stiffness are tested, giving resonance wind velocities in the entire wind velocity range of the wind tunnel.

The analysis considers the following two cross section models:

- Circular cylindrical tube
- Rectangular 1:3 box

For the rectangular box model, the in-line dimension is three times larger than the cross-flow dimension.

3.2 Static wind tunnel rig

To measure the static response in a wind tunnel, a force transducer is placed on the upstream side of the model facilitating measurements of the drag force. Two force transducers are placed at the top to measure the wind-induced lift force and moment. A relatively large mass of the model ensures that the top wires achieve a sufficient pretension such that a positive force is always measured on the top force transducers. The setup is identical on the other side of the wind tunnel, with a similar force transducer placed on the upstream side of the model. A principal sketch of the measurement setup used for static testing is depicted in figure 2.

The output from the calibrated force transducers, knowledge of the model geometry and measurements of the flow velocity allow for the estimation of the static coefficients on the fixed structure. These are defined by the following expressions of the mean drag, lift and moment load per unit length acting on a model

$$F_D = q_m D C_D, \quad F_L = q_m L C_L, \quad F_M = q_m L^2 C_M, \quad (7)$$

where q_m is the mean wind velocity pressure.

Analysing the temporal drag and lift force readings on the nominally non-vibrating model, reveals that the spectral power of the two signals have excess power at certain frequencies. For the lift, this corresponds to the oscillating force caused by vortex shedding, expressed by the Strouhal number for a fixed structure. All results from the static measurements are presented in Sect. 4.1.

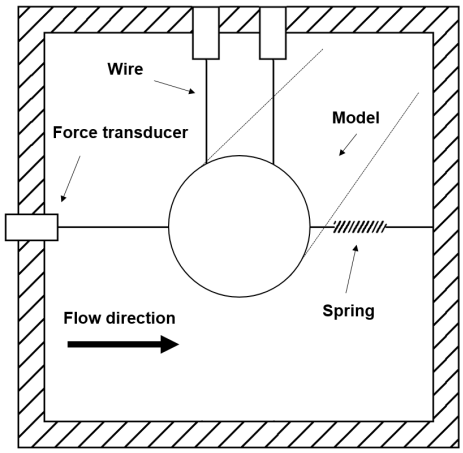

Figure 2: Principal sketch of the measurement setup used for static testing, looking from the side of the wind tunnel. The setup facilitates measurements of the wind-induced drag and lift force and moment. The setup is identical on the other side of the wind tunnel with a force transducer also placed on the upstream side of the model.

3.3 Dynamic wind tunnel rig

To measure the dynamic response, a lightweight model is mounted in the tunnel, constrained in the vertical direction, such that cross-flow deflections are restricted. Initial testing provided evidence that in-line VIV were initialised at wind velocities considerably below those where cross-flow VIV are of relevance, thus the restriction in the vertical direction is used only to provide a stable vertical position of the model in the low-turbulent wind tunnel flow. Any resonant cross-flow forcing can easily be identified by a corresponding loss of tension in the top wires, and all measurements performed under such conditions have been discarded. In the horizontal direction, the model is positioned between springs to achieve a desired oscillation frequency. One spring connects to a force transducer via a string that allows the deflection to be read, by a calibration done prior to beginning the experiment. Note that the US wind tunnel is also equipped with lasers to enable direct measurements of the model deflections. A principal sketch of the measurement setup used for dynamic testing is presented in figure 3. The dynamic measurements allows for a characterisation of the model-specific dynamic behaviour, especially linked to vortex-induced in-line vibrations.

The wind tunnel is set to run at a series of wind velocities whilst measuring the output of the force transducers. Between each measurement, an appropriate run-in time with constant wind velocity ensures that the oscillations have found a constant level. For each wind velocity, the standard deviations of the measured displacements are determined and by assuming a harmonic motion, the corresponding amplitudes are determined by multiplication by the square root of two.

In the dynamic rig, oscillations are measured as functions of different mass ratios, mode shapes and thereby different mass-damping parameters are simulated. Furthermore, decay tests are performed to measure the natural frequency and the damping at zero wind velocities. These data are relevant in the subsequent analysis of the dynamic behaviour of the full-scale structures. Note that the oscil-

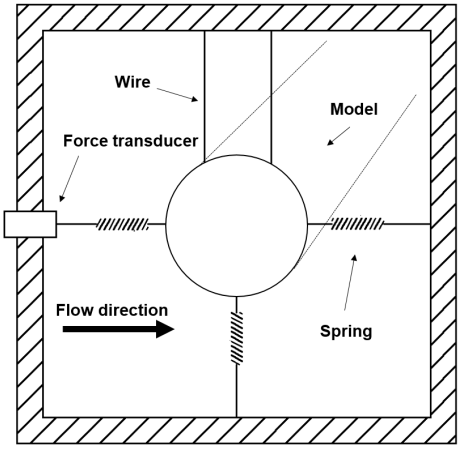

Figure 3: Principal sketch of the measurement setup used for dynamic testing, looking from the side of the wind tunnel. The setup facilitates measurements of an oscillating wind-induced in-line force. The US wind tunnel is also equipped with lasers to enable direct measurements of the model deflections.

lating mass is very different in still air relative to when the models are subjected to flow.

The results from the dynamic response measurements are presented in Sect. 4.2. Furthermore, pressure variations downstream to an in-line oscillating model have been captured using pitot tubes in the US wind tunnel for a single model configurations. This allows for the identification of the different fluid instability regions and therefore also the different physical forcing mechanisms responsible for in-line oscillations. These results are presented in Sect. 4.3.1.

3.4 Model design and construction

The measurements of the static load coefficients do not introduce mass restrictions on the model and readily available robust high-density materials can be in the model construction. In the dynamic wind tunnel rig, the section models are designed to be approximately neutrally buoyant. This may be established by using a low-mass hollow model construction, and replacing the air inside the model with a low-density gas such as helium. The model including suspension will hereby have a mass close to the mass of the displaced air.

The construction of the low-density models required significant engineering and experimentation to meet the structural requirements. The cylindrical models are based on helium-filled cylindrical containers, obtaining additional structural stiffness in part by the internal pressure, but also by using an appropriate chosen shell made by helically wrapped paraffin paper or aluminised polyester. Circular cylindrical models with diameters of 250 mm, 500 mm and 1000 mm have been used for the present analysis.

The rectangular model consists of a carbon fiber rod structure, covered with a light-weight paper-type fabric. Due to the sharp-edged geometry, the use of interior helium filled containers, which attain a cylindrical or spherical shape when inflated, were not found to be convenient in this case. A rectangular model with a cross-flow dimension of 200 mm has been used for the present analysis.

The width of the wind tunnel models are 1.70 m or 2.40 m, using close to the full width of 1.75 m and 2.50 m for the Copenhagen and Vermont wind tunnels, respectively. The height of the wind tunnels are 1.50 m and 3.00 m, respectively. Resonance wind velocities will occur at Reynolds numbers of approximately $10^4 - 10^6$. The possibility of covering both the subcritical and supercritical Reynolds number regime gives a good basis for predicting the behaviour in full scale.

3.5 Blockage effects

A flow occurring in the atmospheric boundary layer or open waters can only to some extent be recreated in an experimental testing facility, due to the finite extent of the generated stream. The spatial limitations may produce several boundary effects which could significantly influence the measurements, i.e. they do not resemble measurements performed in flow conditions without boundary effects. In that sense, it is usually important to consider boundary effects in order to provide a more accurate description of the aerodynamic or hydrodynamic behaviour. However, there is no single established method that takes account for a combination of flow contraction and wall constraints, which are often causing the main blockage effects. In this paper, the data is therefore presented without any correction for blockage, since applying a somewhat heuristic blockage correction expression would produce a data set with a significant level of uncertainty. Also, since most measurements are based on similar model scales, the influence from blockage effects are similar between the measurement series, and the results using different model configurations are therefore often directly comparable. For the 1000 mm diameter circular cylindrical model, the blockage is 33%.

Boundaries causing spatial limitations in the cross-flow direction are known to reduce the amplitude of vortex-induced cross-flow vibrations. This effect is not expected to cause a similar reduction for in-line vibrations, since similar spatial limitations do not exist in the main flow direction.

4 Main results

The static load coefficients and dynamic properties of several cylindrical models are documented in the following section. These originate from a number of different wind tunnel flow situations, where the in-line dynamics are evaluated exclusively for low mass ratio models. In this setting, the physical flow characteristics causing the two in-line vortex-induced fluid instability regions have been measured and identified using recordings of spatial and temporal downstream fluid pressure variations. Additionally, the risk of galloping and torsional structural instability have been assessed by evaluating the static load coefficients for different inclination angles.

4.1 Static load coefficients – nominally non-vibrating models

Drag, lift and moment coefficients for a circular cylindrical model without end plates have been measured in a wind

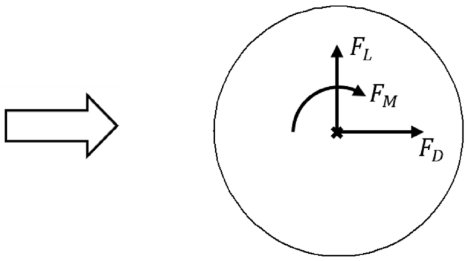

Figure 4: Sign convention of static forces and moments, here shown for the circular cross section. The flow is from left to right.

Table 1: Calculated static load coefficients of the two section models for a zero degree inclination of the approaching flow in the listed Reynolds number regime.

Cross section	C_D	C_L	C_M	St	Re
Circular	0.93	-0.07	-0.01	0.18	4×10^4
Rectangular	1.27	0.01	-0.02	0.05	1×10^5

environment corresponding to $Re \approx 4 \times 10^4$ in the Copenhagen wind tunnel. In the wind tunnel in Vermont, similar measurements have been performed on the rectangular 1:3 cross section model in a flow corresponding to $Re \approx 1 \times 10^5$. The results are listed in table 1, where the static load coefficients are presented according to the definitions stated in Sect. 3.2. The diameter of the circular cylindrical model is 250 mm and the cross-flow and in-line dimensions are 500 mm and 1500 mm, respectively, for the rectangular model. The sign convention of static forces and moments is presented in figure 4.

The drag coefficient of a circular cylinder without free-end flow in the relevant Reynolds number regime is specified to be $C_{D,0} = 1.2$ [16]. In the wind tunnel setup, free-end flow exists, but is somewhat limited due to the close proximity of the side walls. The measured drag coefficient is approximately 20% smaller than this value, which is in good agreement with the presence of a limited free-end flow. Note that the drag coefficient of this section model depends on the Reynolds number regime.

The drag coefficient of a sharp-cornered rectangular cross section without free-end flow is stated in the Eurocode 1 specifications [17]. For a ratio of the cross-flow and in-line dimension of 1:3 a drag coefficient of $C_{D,0} = 1.36$ is specified. The measured drag coefficient is approximately 7% smaller than the specified value, which again is in good agreement with the presence of a limited free-end flow. Note that the drag coefficient for a sharp edged section does not depend on the Reynolds number regime.

The lift and moment coefficients are theoretically both zero due to the symmetry of the cross sections considered; thus, the measured responses of negligible magnitudes are entirely due to very small fluctuations in the wind flow, model imperfections and minor measurement uncertainties.

By analysing the spectral power density function, the lift force signals are found to have distinct peaks caused by vortex shedding. For each cross section model, this procedure allows for the estimation of the Strouhal number for the fixed structure, as listed in table 1.

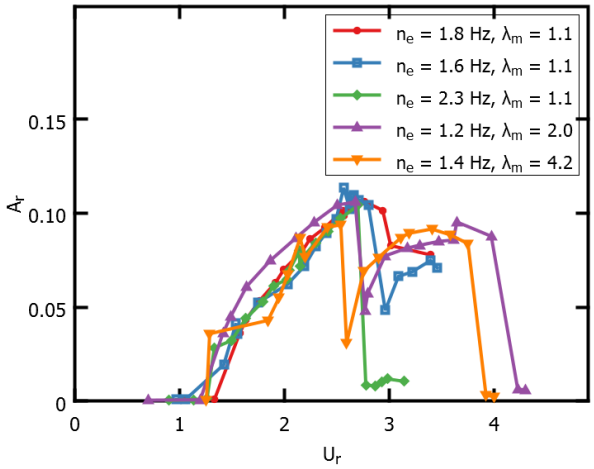

Figure 5: Measured response of five model cylinders configurations in steady air as function of the reduced wind velocity for different model configurations oscillating in a uniform mode shape. The flow conditions correspond to $1 \times 10^4 \leq Re \leq 3 \times 10^4$.

4.2 Vortex-induced in-line vibrations in steady flow – vibrating models

Vortex-induced in-line vibrations in steady flow have been measured on several experiemental configurations, corresponding to differences in model mass ratio, natural frequency, mode shape and Reynolds number regime.

4.2.1 *Circular cylindrical model - Mass ratio and natural frequency*

The dynamic in-line response has been measured on five configurations of a 250 mm diameter cylinder model in flow conditions corresponding to $1 \times 10^4 \leq Re \leq 3 \times 10^4$, see figure 5. For these experiments, the model was set to oscillate in a uniform mode shape and the model was equipped with end plates to limit the disturbance caused by end effects.

A precise estimation of the mass-damping parameter is not possible, since the structural damping is not straightforward to determine. However, for these models the mass-damping parameter scales with the mass ratio. Assuming a structural damping of $\delta_s = 0.03$, the mass-damping parameter is $Sc_G \approx 0.12$ for $\lambda_m = 1.1$.

The onset of the first fluid instability region is located at $U_r \approx 1.1$ for all five configurations, while the maximum amplitude, being approximately 11% of the cylinder diameter for the mass ratios $\lambda_m = 1.1$ and $\lambda_m = 2.0$, is only slightly reduced for the larger mass ratio of $\lambda_m = 4.2$. The shift between the first and second fluid instability seems to depend on the mass ratio as well. For larger mass ratios, corresponding to a larger stability parameter, the response drops at slightly smaller reduced wind velocities, which is in accordance with the DNV response model.

A change in the natural frequency of the model does not seem to influence the characteristics of the response in the first fluid instability region, justifying the use of the reduced fluid velocity as a descriptive parameter. For all configurations, the maximum response occurs in the

range $2 < U_r < 3$, which fits well with the previously presented in-line response models. Also, by increasing the mass ratio, the maximum response seems to occur at slightly smaller reduced wind velocities.

The second fluid instability responses for $\lambda_m = 2.0$ and $\lambda_m = 4.2$ are similar, being slightly smaller in maximum amplitude for $\lambda_m = 4.2$. For the models with a mass ratio of $\lambda_m = 1.1$, the model begins to buckle and deform at reduced wind velocities above $U_r \approx 3$. When this happens, the tests are stopped because the mode shapes are no longer uniform. As a result, the second fluid instability region is not fully characterised by the models with the lowest mass ratio.

4.2.2 *Circular cylindrical model - Mode shape*

For a cylindrical 250 mm diameter model, the influence of the mode shape on the in-line vibrations has been investigated for two model configurations, see figure 6. In these measurements, the flow conditions correspond to $1 \times 10^4 \leq Re \leq 3 \times 10^4$.

The cylindrical model is oscillating with an amplitude of around 15% of the cylinder diameter for a free-end mode shape, somewhat larger than the amplitude found for models oscillating in a uniform mode shape, see figure 5. The difference in the amplitude between the mode shapes can likely be explained by a different scaling of positive and negative fluid dynamic damping effects along the structure. This phenomenon is actually well-known for cross-flow VIV [18].

Attaching additional mass to the free end of the cylinder increases the mass-damping parameter and decreases the maximum amplitude of the oscillations to around 10% of the cylinder diameter. Also, note that the second fluid instability region ($U_r \approx 3$) apparently does not give a distinct response in this mass-damping range for a free-end mode shape. The fact that the mass is added to the free end of the model implies that the mass-damping is increased relatively more than the mass ratio listed in the legend on figure 6. Assuming a structural damping of $\delta_s = 0.03$, the mass-damping parameters are $S c_G \approx 0.17$ and $S c_G \approx 0.30$ for the two presented model configurations.

4.2.3 *Circular cylindrical model - Reynolds number*

Dynamic response characteristics in flow conditions corresponding to higher Reynolds numbers, can be obtained in a wind tunnel by increasing the model dimensions or by increasing the wind velocity. Both approaches imply considerable challenges for the model structure. A larger model dimension naturally implies increased sag and bending moments, and the present low mass ratio requirements would often result in a model which is less likely to withstand higher velocities without deformations or similar undesirable effects. Nevertheless, response measurements in even higher Reynolds number regimes have been obtained using a large inflatable scale model, having a diameter of 1000 mm. The responses of four such configurations in high Reynolds number regimes are presented in figure 7. For these four configurations, the mass ratio is held approximately constant and the model was equipped with end plates to limit the disturbance caused by end effects.

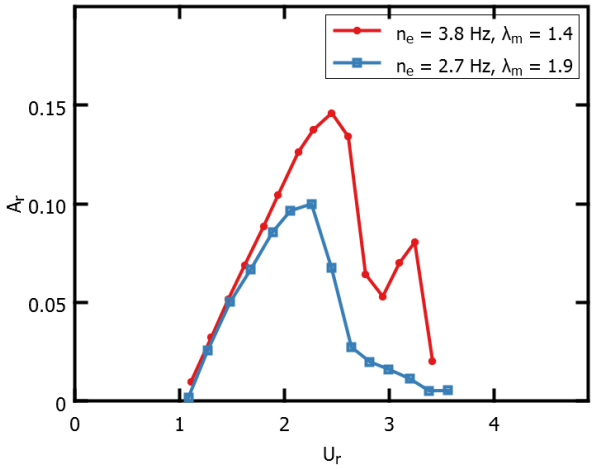

Figure 6: Measured in-line response of a cylindrical model as function of the reduced wind velocity for two different configurations oscillating in a free-end mode shape. The maximum response depends on the mode shape (compare to figure 5) and is reduced when a large mass is added. The flow conditions correspond to $2 \times 10^4 \leq Re \leq 4 \times 10^4$.

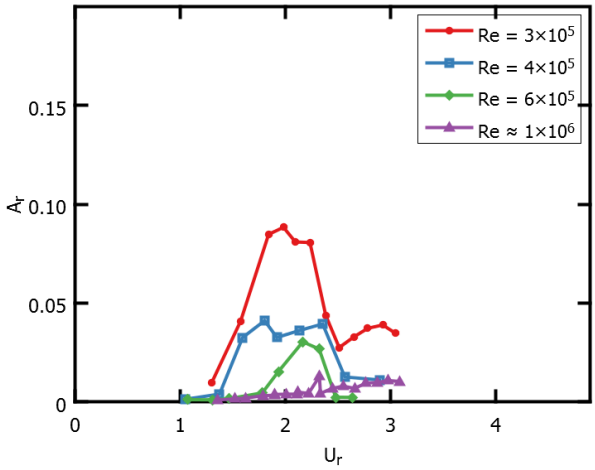

Figure 7: Measured in-line response of a 1000 mm diameter model cylinder in steady air as a function of the reduced wind velocity for different Reynold number flow regimes.

For $Re = 3 \times 10^5$, the model is seen to have an in-line response amplitude of up to 9% of the cylinder diameter and two visible fluid instability regions. A single fluid instability region with a much reduced response is observed for $Re = 4 \times 10^5$ and $Re = 6 \times 10^5$, and for the latter flow regime, non-uniform oscillations were observed for reduced wind velocities larger than $U_r \approx 2.2$. For the flow regime corresponding to $Re = 1 \times 10^6$, no clear indication of in-line fluid instabilities is observed and the response is just slowly increasing with wind velocity. The only exception is a single peak at $U_r \approx 2.3$ corresponding to an amplitude of around 1% of the cylinder diameter.

The maximum response, as well as the velocity interval in which oscillations occur, are seen to be significantly reduced for increasing Reynolds numbers. This general trend is most likely not entirely caused by the change in the flow regime characteristics with the increasing Reynolds num-

ber, but is also due to related side effects of the increased wind velocity, such as an increased deformation force of the wind tunnel model, and an associated increased energy dissipation in the complete oscillating system. However, it is reasonable to assume that no significant amplification of the overall response would happen as a result of the change in the flow regime for the Reynolds numbers considered. Note also that, as stated previously, wind tunnel blockage is not accounted for in the presented data; thus the reduced wind velocities, and thereby also the Reynold numbers, are slightly underestimated.

The physical mechanisms responsible for in-line vibrations is a certain combination of forcing due to vortex-shedding and a related change in the aerodynamic damping in the direction of the flow. Exactly the same physical mechanisms working in the cross-flow direction are responsible for cross-flow VIV. In the latter case, a change in aerodynamic damping is responsible for the transition range at which the smaller deflections governed by lift forces changes to larger deflections governed by motion-induced forces. The location of the transition is described by the aerodynamic damping factor for cross-flow amplitudes [11]. The presence of large cross-flow deflections governed by motion-induced forces therefore depends on the aerodynamic damping factor which in turn depends on Reynolds number. Since the physical mechanisms responsible for vibrations are similar in the in-line and cross-flow directions, it is expected that the maximum amplitudes of in-line oscillations show a similar dependence on the aerodynamic damping through the Reynolds number. For cross-flow oscillations, the aerodynamic damping factor attains its minimum at $Re \approx 6 \times 10^5$ according to Eurocode 1 specifications [17], which implies that in this range only small deflections governed by lift forces are to be expected. Apparently, a similar tendency is true for in-line oscillations.

4.2.4 *Rectangular model*

In contrast to the previously tested cylindrical models, the geometry of the rectangular cross section requires that the model is constructed using a lightweight skeleton structure, since the sharp-edged geometry cannot be obtained by pressurised balloons alone. This implies that a mass ratio very close to one is very difficult, if not impossible, to obtain with the model dimension of $D = 200$ mm related to the present wind tunnel testing. Therefore, the smallest mass ratios considered for the rectangular section model are larger than those related to the cylindrical models. A plot of the measured normalised response amplitudes as a function of the reduced wind velocity is presented in figure 8. The flow conditions correspond to $Re \approx 2 \times 10^4$. Again, for these models the mass-damping parameter scales with the mass ratio. Assuming a structural damping of $\delta_s = 0.03$, the mass-damping parameter is $S\,c_G \approx 0.20$ for $\lambda_m = 2.2$.

The presented results show that the rectangular cross section apparently is much less prone to in-line vortex-induced oscillations than the cylindrical cross section. The maximum amplitude is below 2% of the cross-flow dimension, and there is actually a slight increase in amplitude with increasing mass ratio for the four presented model configurations. Note that only a single fluid instability region is visible, located at approximately $3 \leq U_r \leq 4$.

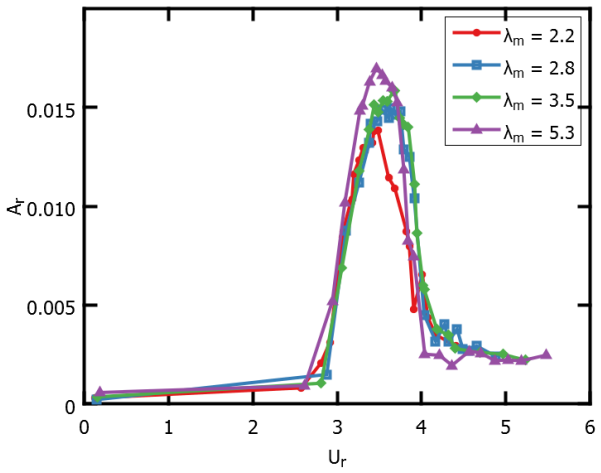

Figure 8: Reduced amplitudes of the rectangular section model for different mass ratios. The largest amplitude is below 2% of the cross-flow dimension. For all model configurations, a clear in-line model response is only seen for wind velocities corresponding to approximately $3 \leq U_r \leq 4$.

The aerodynamic damping for the rectangular cross section is larger than for circular cross sections, simply due to the larger drag coefficient and the fact that a higher reduced wind velocity is necessary to initialise the oscillations. This effect is also relatively more pronounced at small mass ratios at similar reduced wind velocities. It is deemed that this effect is responsible for the limited in-line response. The decrease in aerodynamic damping with increasing model mass could also account for the slight increase in maximum response for larger mass ratios.

The initialisation of the in-line vortex-induced forcing is related to the Strouhal number for the fixed structure. For the rectangular model and the cylindrical model, the ratio of the measured Strouhal numbers for the fixed structures are approximately 3.6, see table 1, implying an onset of the in-line forcing frequency relative to the structural eigenfrequency at three to four times higher wind velocities for the rectangular model. This is in agreement with the onset of the in-line vortex-induced forcing close to the structural eigenfrequency at $U_r \approx 3$, which is three times larger than the onset found for the cylindrical models, see Sect. 4.2.1.

As seen on figure 8, the in-line vibrational behaviour was investigated for reduced wind velocities up to approximately $U_r = 5$. For a similar 1:3 section model, torsional vortex-induced oscillations in air have been reported to have an onset near $U_r = 6.5$ [19]. This is approximately twice the reduced velocity at which the in-line oscillations were seen to attain the largest amplitudes, which suggests that the in-line oscillations measured on the rectangular section model are caused by a normal asymmetric vortex shedding pattern.

4.3 Additional investigations

Several experiments have been performed in addition to the investigations of model-specific static and dynamic load

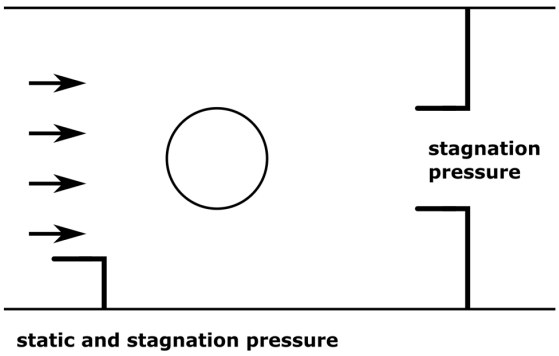

Figure 9: Sketch of the model setup capturing the downstream pressure variations due to vortex shedding. Two downstream pitot tubes are used to capture the spatial information needed to distinguish between asymmetric and symmetric vortex shedding.

characteristics. In this section some supplementary findings are listed, which confirms or enlightens the previously documented results linking in-line vortex-induced vibrations to basic flow characteristics, and the fluid-dynamical and structural parameters.

4.3.1 *Identification of fluid instability regions*

As mentioned in Sect. 2, the mechanism responsible for the first fluid instability causing in-line oscillations is regular, alternating vortex shedding combined with a secondary, symmetric vortex shedding pattern which occurs as a result of in-line structural motion relative to the fluid. In the second fluid instability region, the forcing is entirely due to regular vortex shedding from alternating sides of the cylinder. Therefore, the two types of in-line responses are caused by downstream pressure variations oscillating with three and two times the Strouhal frequency, respectively. Measurements of the spatial and temporal downstream pressure variations could therefore be used to identify the forcing mechanism; thus, identifying the corresponding fluid instability regions.

In the US wind tunnel, the downstream pressure variations have been captured using two pitot tubes located approximately 750 mm behind a 500 mm diameter cylindrical model oscillating in the in-line direction, having an eigenfrequency of $n_s \approx 2.7$ Hz. The pitot tubes are vertically aligned with the model top and bottom, see figure 9. The probes are 8 mm diameter NPL type pitot-static tubes with ellipsoidal head complying with ISO 3966. The dynamic pressure sensors have a response time of less than 10 ms, and the setup can easily capture the generated pressure fluctuations. Hot-wire anemometers which are often used to capture high frequency flow fluctuations are therefore not required in the present case.

When model oscillations couple with vortex shedding, the eigenfrequency of the model becomes visible in the power spectra of the measured time series of pressure variations at the two downstream pitot tubes. Figures 10 and 11 illustrate such spectral power densities at $U_r = 2.16$ and $U_r = 3.26$, respectively.

In the first fluid instability region, the vortex shedding pattern is complex as it is a mix of both alternating and

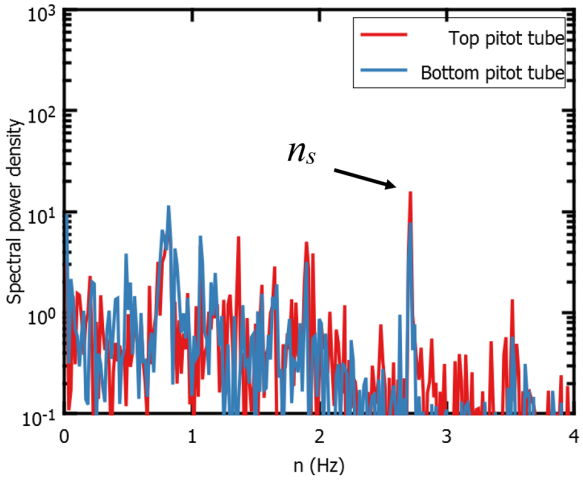

Figure 10: Spectral power density of the top and bottom pitot tube pressures at $U_r = 2.16$, in the first fluid instability region, indicating a clear peak at the models natural frequency n_s.

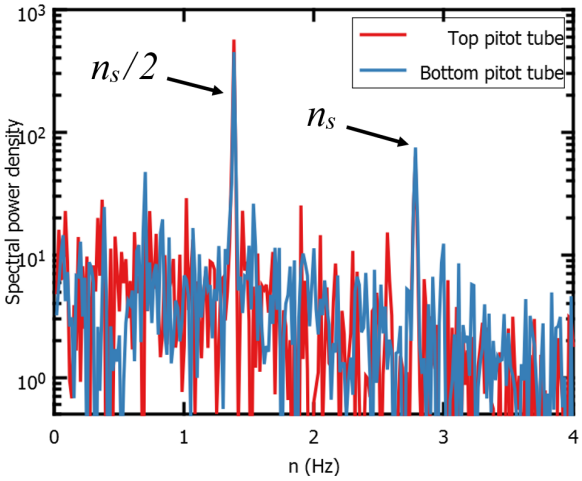

Figure 11: Spectral power density of the top and bottom pitot tube pressures at $U_r = 3.26$, in the second fluid instability region, indicating clear peaks at both the models natural frequency n_s and at $n_s/2$.

symmetric vortex shedding. In general terms, it can be divided in two sub-regions:

– For relatively low reduced wind velocities ($U_r \approx 1$), the cross-correlation of the two signals are dominated by correlation peaks of a period T, here defined as the inverse of the model eigenfrequency of approx. 2.7 Hz. This indicates that symmetric vortices, which are highly correlated in the wake, are shed with the motion of the model. Concurrently, correlation at zero time lag exists, but maximum correlation is not achieved here due to the occasional alternating vortex pair. By lowering the wind velocity, the vortex shedding becomes increasingly dominated by symmetric pairs, and the model eigenfrequency becomes visible while half the model eigenfrequency disappears from the spectra.
Depending of the model natural frequency, the regular asymmetric vortex shedding on a fixed cylinder corresponding to a Strouhal number of $St = 0.18$ may be-

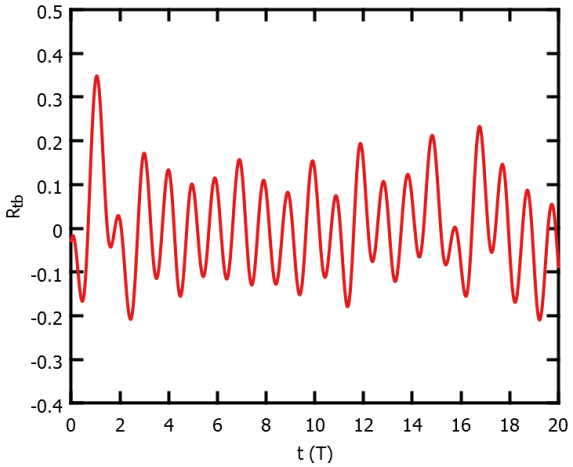

Figure 12: The cross-correlation between top and bottom pitot pressures at $U_r = 2.16$, indicating a mix of symmetric and regular, asymmetric vortex shedding.

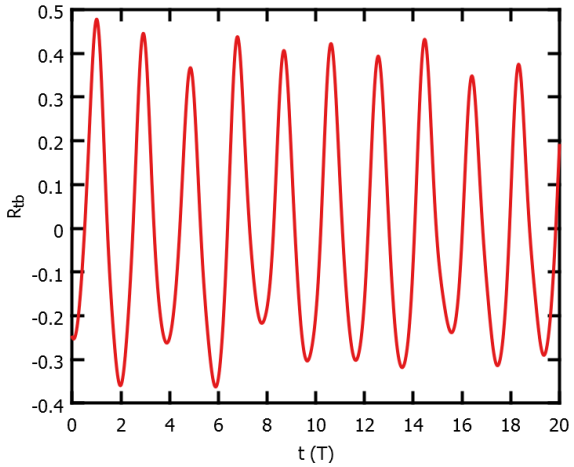

Figure 13: The cross-correlation between top and bottom pitot pressures at $U_r = 3.26$, indicating regular, asymmetric vortex shedding.

come apparent at reduced wind velocities below, and in, the first part of the first fluid instability region where very little or no response of the model is observed.

– At higher reduced wind velocities ($U_r \approx 2$), the cross-correlation is approximately sinusoidal, with some irregularities and a slight decay of the peak correlations for increased time lag, see figure 12. At $U_r = 2.16$, the first peak of correlation occurs at $t = T$ and reoccurs with period $2T$. This indicates that the vortex shedding is predominantly alternating. The correlation also show a smaller sinusoidal component, positive at $t = 0$ s with period T, indicating symmetric vortex shedding. Half the model eigenfrequency is not visible in the corresponding spectra, distinguishing this region from the second fluid instability region, see figures 10 and 11.

The second fluid instability region is due to vortex shedding from alternating sides as is familiar on fixed cylinders. This region is characterised by the appearance of peaks in the spectrum at the model eigenfrequency and at half the model eigenfrequency, see figure 11. This suggests that vortices are shed once per model oscillation, as the spectral footprint consists of the frequency by which each single vortex is shed, and also the frequency corresponding to the shedding of a full period of a pair of vortices. If the pitot pressures are subtracted from each other the resulting spectrum reveals no significant contribution at the frequency corresponding to the model eigenfrequency. If the signals are added a clear peak at the model eigenfrequency occurs in the corresponding spectrum. The cross-correlation on figure 13 of this shedding type is approximately sinusoidal with periodic peaks of constant value indicating a long time correlation. The period is $2T$, twice the period of the model oscillations, with the first peak correlation at T consolidating the alternating nature of the shedding.

Between the two fluid instability regions, the cross-correlation of the two pitot pressures remains sinusoidal with a period of $2T$, but the level of correlation decays quickly. The model eigenfrequency leaves very little footprint in the frequency spectra while half the eigenfrequency remains visible.

Measurements of the spatial and temporal downstream pressure variations on an in-line oscillating cylindrical model therefore allows for the identification of the first and second fluid instability region; thus, identifying the corresponding forcing mechanism causing in-line structural oscillations in stationary fluid flow. The investigation verifies that the physical phenomena responsible for vortex-induced vibrations in air are similar as those reported in water [10].

4.3.2 *Structural instability phenomena*

The angular dependence of the static load coefficients may be used not only to predict fluid-induced forces, but also to investigate if the cross section is susceptible to aeroelastic or hydroelastic structural instability phenomena such as galloping and flutter. For this, the Scruton number, of the more general non-dimensional mass-damping parameter, may be used in predictions of cross-flow galloping, assuming a driving force proportional to the in-line dimension. The rotational structural response can be modelled by a one degree of freedom system with a torsional forcing determined by the fluid-induced moment load. It is a standard approach to consider a linearisation argument to indicate that two types of structural instabilities can occur; one being torsional galloping and one being static divergence [20].

Due to the geometrical symmetry, galloping and torsional structural stability are not relevant for the circular cross section model. For the rectangular cross section, a negative slope of the aerodynamic lift was measured, implying that cross-flow galloping vibrations might exist for small inclinations of the flow due to unstable aerodynamic loading conditions. The aerodynamic moment has a negative slope for small inclinations. This implies that the structure is stable towards flow-induced excessive twist. However, a negative slope is known to increase the risk of torsional galloping, due to negative aerodynamic damping effects.

The slope of the moment coefficients for rectangular sections rotating about the geometric center have previously been reported for 1:2 and 1:4 cross sections in the literature, being -0.64 and -18, respectively, for α measured in radians, but using the cross-flow dimension as the characteristic dimension in the definition of the moment load

per unit length [21]. For the analysed 1:3 cross section, the measurements suggest $\frac{dC_M}{d\alpha}|_{\alpha=0} \approx -1.1$, corresponding to a value of -9.9 using the cross-flow dimension as the characteristic dimension.

5 Discussion

For free-span circular cross-section pipelines submerged in water, the DNV in-line response model gives an empirical description in current dominated full-scale conditions. The presented results indicate that the maximum in-line response of a close to neutrally buoyant circular cylindrical model oscillating in a uniform mode shape in air is well-described by the DNV model, both in terms of maximum response and the reduced velocities at which in-line VIV is relevant. The dependence on the stability parameter expressed in the DNV model cannot be confirmed based on the conducted measurements, since a precise estimation of the total damping, or in particular the aerodynamic damping, is not straightforward. However, the overall tendency of a reduction in the maximum response occurring at a lower reduced flow velocity when increasing the stability parameter, or in the present case increasing the mass ratio, is indeed observed in the measured responses.

In the performed dynamic testing, models with a mass ratio in the range of, say, 1.0 – 2.0 of the surrounding fluid, apparently produce a comparable maximum response for a uniform mode shape. In other words, the related Scruton curve has a small slope near zero. This observation can be used as a guidance for future testing, since it implies that maximum responses might be correctly estimated using models which are only close to being neutrally buoyant.

Based on additional measurements in flow conditions corresponding to $10^5 \leq Re \leq 10^6$, it is reasonable to assume that no significant amplification of the overall response would happen as a result of the change in the flow regime for the Reynolds numbers considered. A compensation for the slightly lower Reynolds number in the wind tunnel environment compared to full scale conditions, is therefore likely not necessary to be included in the safety requirements. Nevertheless, subsequent wind tunnel measurements at even higher Reynolds numbers could potentially provide additional insight into the importance of this topic.

Measuring the spatial and temporal downstream pressure variations on an in-line oscillating cylindrical model allowed for the identification of the first- and second fluid instability region, thus identifying the forcing mechanism causing in-line structural oscillations in steady fluid flow. The investigation verified that the physical phenomena responsible for vortex-induced vibrations in air are similar as those reported in water [10].

The rectangular cross section is apparently much less sensitive to in-line VIV than the cylindrical cross sections, likely caused by a larger fluid-dynamic damping. The onset of in-line VIV happens at larger reduced velocities, probably due to the smaller Strouhal number for the structure.

6 Conclusion

The presented results provide a preliminary insight into a fundamental methodology for the transfer of certain aerodynamic actions to equivalent hydrodynamic actions, related to both static response characteristics and in-line vibrations caused by vortex shedding. A consistency between the results obtained in the wind testing facilities at Svend Ole Hansen ApS and SOH Wind Engineering LLC, and results published by others were observed; thus, verifying the understanding of the general dynamic properties of low mass ratio structures and the type of physical phenomena which are of relevance for the in-line structural oscillations in steady fluid flow. This consistency was found on both the qualitative and quantitative levels, giving a response of similar magnitude for experimental configurations corresponding to comparable basic flow characteristics and model parameters. In this sense, the wind tunnel testing has turned out to be a very economical and powerful tool for determining and verifying hydrodynamic data.

It is of fundamental interest that wind tunnel experiments have shown that in-line VIV caused by steady winds on model structures with a density comparable to air, and the response prescribed on neutrally buoyant structures in water are of very similar nature. As this is a very wide-ranging field, the presented work cover basic principles and demonstrates prevailing tendencies. The conversion of model-scale results to full-scale predictions should therefore be assessed accordingly and the interpretation of the presented model-scale data should focus on the fact that the basic physical mechanism generating the in-line vibrations in question are equivalent in model scale and full scale, and in air and water. Nonetheless, the presented model tests have provided clear indications of the static and dynamic properties of specific neutrally buoyant structures and should form a basis for future systematic investigations providing in-depth descriptions on the flow-induced structural behavior.

The authors would like to thank Ph.D. candidate Andreas Saur Brandtsegg from Dr.techn.Olav Olsen AS and the Norwegian Institute of Technology (NTNU), and Professor Odd Faltinsen from NTNU for valuable advice and expertise. A special thanks also goes to the employees at Svend Ole Hansen ApS, SOH Wind Engineering LLC, Reinertsen AS, Dr.techn.Olav Olsen AS and the Norwegian Public Roads Administration.

References

1. R. King, Ocean Engineering **4**, 141-171 (1977)
2. T. Sarpkaya, Journal of Applied Mechanics **46**, 241-258 (1979)
3. P. W. Bearman, Annual Review of Fluid Mechanics **16**, 195-222 (1984)
4. M. M. Zdravkovich, Journal of Fluids Engineering **99**, 618-633 (1977)
5. C. Mannini, A.M. Marra, G. Bartoli, Journal of Wind Engineering and Industrial Aerodynamics **132**, 109-124 (2014)
6. M. Belloni, S.Giappino, S. Morganti, S. Muggiasca, A. Zasso, Ocean Engineering **94**, 140-154 (2014)

7. C. C. Feng, *The measurement of vortex-induced effects in flow past stationary and oscillating circular and D-section cylinders* (Master's Thesis, University of British Columbia, Vancouver, B. C., Canada, 1968)
8. M.H. Bahmani, M.H. Akbari, Ocean Engineering **37**, 511-519 (2010)
9. S. E. Ramberg, O. M. Griffin, Proceedings of Hydrodynamics in Ocean Engineering, 1223-1245 (1981)
10. B. M. Sumer, J. Fredsøe, *Hydrodynamics Around Cylindrical Structures*, (World Scientific, 2006)
11. S. O. Hansen, Proceedings of the Institution of Civil Engineers - Structures and Buildings **166**, 560-571 (2013)
12. A. Khalak, C. H. K. Williamson, Journal of Fluids and Structures **13**, 813- 851 (1999)
13. R. King, *Vortex excited structural oscillations of a circular cylinder in flowing water* (PhD Thesis, Loughborough University, 1974)
14. Det Norske Veritas, *Recommended Practice - Free Spanning Pipelines DNV-RP-F105* (Det Norske Veritas, 2006)
15. H. Braaten, H. Lie, M. Søreide, S. Svardal, Proceedings of the 26th International Conference on Offshore Mechanics and Arctic Engineering, (2007)
16. C. Dyrbye, S. O. Hansen, *SBI-Anvisning 158 - Vindlast på bærende konstruktioner*, (Statens Byggeforskningsinstitut, 1989)
17. DS/EN 1991-1-4:2007: Eurocode 1, *Actions on structures - Part 1-4: General actions - Wind actions*, (Dansk Standard, 2007)
18. S. O. Hansen, Proceedings of the third Structural Engineers World Congress, (2007)
19. K. Washizu, A. Ohya, Y. Otsuki, K. Fujii, Journal of Sound and Vibration **72**, no. 4, 507-521, (1980).
20. C. Dyrbye, S. O. Hansen, *Wind loads on structures* (John Wiley & Sons Ltd., 1997)
21. M. P. Païdoussis, S. J. Price, E. de Langre, *Fluid-Structure Interactions: Cross-Flow-Induced Instabilities* (Cambridge University Press, 2010)